Multifunctional Magnetic Nanoparticles for Dual Applications in Hyperthermia and MRI Contrast Enhancement: In-Vitro Evaluation and Biocompatibility

Tej Kumar

Research Scholar, Department of Physics, Radha Govind University, Ramgarh, Jharkhand.

ABSTRACT

Background:

Magnetic nanoparticles (MNPs) have been touted as theranostic hopefuls with therapeutic and diagnostic modalities like magnetic hyperthermia and magnetic resonance imaging (MRI). They are well suited for targeted cancer treatment and diagnosis due to their capacity for localized heating and magnetic resonance contrast enhancement.

Objective:

The aim of this research is to prepare, characterize, and assess PEG/Dextran-coated superparamagnetic iron oxide nanoparticles (Fe_3O_4) for their bimodal functionality in magnetic hyperthermia and MRI contrast agent application and cytocompatibility.

Methods:

Fe_3O_4 nanoparticles were prepared through a controlled co-precipitation process under nitrogen gas and then surface-modified with PEG and dextran to enhance biocompatibility and colloidal stability. Structural, morphological, and magnetic properties were evaluated through XRD, TEM, FTIR, DLS, and VSM. Hyperthermia efficacy was assessed under an alternating magnetic field (400 kHz, 20 mT) via specific absorption rate (SAR) analysis, and MRI contrast performance was assessed from T_2 relaxivity (r_2) measurements. In-vitro cytotoxicity against HeLa and MCF-7 cell lines was assessed using the MTT assay.

Results:

The nanoparticles had an evenly spherical morphology (~12 nm), superparamagnetic properties (Ms = 68.4 emu/g), and very good colloidal stability ($\zeta = -23.8$ mV). There was a high heating response with an SAR of 165 W/g Fe, and the T_2 relaxivity was very high at 47.5 $s^{-1} \cdot mM^{-1}$, outperforming commercial Resovist®. Cell viability tests supported more than 80% cell viability up to 200 µg/mL, showing good biocompatibility.

Conclusion:

The PEG/Dextran-coated Fe_3O_4 nanoparticles exhibited superior MRI contrast enhancement and effective hyperthermia performance, which justified their use as safe and efficient multifunctional nanotheranostic agents for targeted cancer therapy.

Keywords: *Magnetic nanoparticles (MNPs); Superparamagnetic iron oxide nanoparticles (SPIONs); PEG/Dextran coating; Co-precipitation synthesis; Surface functionalization; Physicochemical characterization; Magnetic hyperthermia; Specific absorption rate (SAR); MRI relaxivity (r_2); Cytotoxicity assay (MTT); Biocompatibility; Nanotheranostics; Dual-function imaging and therapy; Results and performance evaluation.*

1. Introduction

The phenomenal growth of nanotechnology has transformed the areas of biomedical diagnostics and cancer treatment by making it possible to engineer materials at the nanoscale with controlled physical and chemical attributes(Hu et al., 2009). Of the numerous applications, nanotechnology has been instrumental in transforming cancer diagnosis and treatment with new solutions for early detection, targeted drug delivery, and minimally invasive therapeutic interventions(Kaszuba et al., 2010). Particularly, magnetic nanoparticles (MNPs) have become potent devices in the field of biomedical imaging and cancer theranostics due to their distinctive magnetic, optical, and surface modification features to play a variety of functions all at once(Prokopiou et al., 2021). Incorporation of nanomaterials into imaging devices has greatly increased sensitivity, resolution, and specificity to make real-time monitoring of disease state and therapeutic response possible(Okamoto et al., 2017).

In contemporary medical imaging, non-invasive modalities including Magnetic Resonance Imaging (MRI), Positron Emission Tomography (PET), and Computed Tomography (CT) are indispensable diagnostic methods(Busquets et al., 2015). MRI, in special, is preferred because of its high soft tissue contrast, high spatial resolution, and lack of ionizing radiation(Pradhan et al., 2007). These imaging modalities have significantly contributed to early cancer detection and diagnosis, allowing clinicians to visualize tumor morphology and physiological alterations in vivo(Minaei et al., 2019). Yet, in spite of their utility, the performance of these methods greatly relies on the availability of contrast agents that can make structures within the body more visible(Nan et al., 2017). Hence, creating safe, effective, and multifunctional contrast agents is a challenge to overcoming the accuracy of diagnostic imaging(Sheng et al., 2018).

One of the serious drawbacks of traditional contrast agents, particularly gadolinium-based agents, is their risk of toxicity and limited biological half-life(Mohammadi et al., 2023). Gadolinium has the potential to accumulate in tissues and induce nephrogenic systemic fibrosis in patients with renal insufficiency(Rego et al., 2020). Furthermore, these agents are usually not stable, non-specifically biodistribute, and do not possess multifunctionality, restricting their application for concurrent diagnosis and therapy(Negri et al., 2025). This has created a pressing demand for biocompatible and non-toxic substitutes that can offer both diagnostic and therapeutic functions within one nanosystem — a strategy now widely known as theranostics (Fahim et al., 2025).

Objective

To synthesize, characterize, and assess multifunctional magnetic nanoparticles (MNPs) having optimized structural, magnetic, and biocompatible features for dual uses in MRI contrast enhancement and magnetic hyperthermia.

Specific Goals:

- To prepare SPION-based nanoparticles with a controlled size, shape, and magnetic saturation.
- To study their magnetic, thermal, and relaxometric performance for imaging and therapeutic purposes.
- To evaluate their cytocompatibility and in-vitro hyperthermic activity against cancer cell lines.

Hypothesis

H1: Surface-modified Superparamagnetic Iron Oxide Nanoparticles (SPIONs) will exhibit better MRI contrast performance based on greater magnetic responsiveness and maximal T_2 relaxivity compared to standard gadolinium-based contrast agents.

H2: The same surface-engineered SPIONs will also display effective localized heat generation in an alternating magnetic field (AMF), thus effectively inducing magnetic hyperthermia for effective targeted tumor ablation with little cytotoxicity to normal cells.

2. Literature Review

Magnetic nanoparticles (MNPs) such as superparamagnetic iron oxide nanoparticles (SPIONs) have proved to be multifunctional platforms for concurrent cancer diagnosis and treatment due to their inherent magnetic, optical, and biocompatibility properties(Xu et al., 2017). Traditional gadolinium-based MRI contrast agents tend to be toxic, and SPIONs have therefore been researched as less harmful, more effective alternatives with controllable surface chemistry(Ereath Beeran et al., 2019). Synthesis and surface modification advancements—through the application of polymers such as PEG, dextran, and chitosan—have allowed for enhanced stability, bioavailability, and targeted drug delivery to tumor tissue. The nanoparticles not only provide enhanced T_2-weighted MRI contrast but also produce local heating upon exposure to an alternating magnetic field, allowing for magnetic hyperthermia of tumors. Furthermore, their enzyme-mimicking "nanozyme" functions have been exploited for biosensing and diagnostics assays. Various formulations like Resovist® and Ferumoxytol have entered clinical trials, indicating their translational worth. Yet, maximizing magnetic heating efficacy, reducing off-target deposition, and maintaining long-term biocompatibility remain essential issues for clinical application(Pucci et al., 2022).

3. Methodology

3.1 Materials

Ferric chloride hexahydrate ($FeCl_3 \cdot 6H_2O$) and ferrous sulfate heptahydrate ($FeSO_4 \cdot 7H_2O$) of ≥99% purity were purchased from Sigma-Aldrich and used as starting materials for nanoparticle synthesis. Polyethylene glycol (PEG-2000), dextran (MW ~40 kDa), and ammonium hydroxide (NH_4OH, 25%) were used without purification. Dulbecco's Modified Eagle's Medium (DMEM), fetal bovine serum (FBS), and MTT reagent needed for cytotoxicity assays were purchased from HiMedia Laboratories. All reagents and solutions were prepared in high-purity deionized (DI) water having a resistivity of 18.2 MΩ·cm to provide experimental accuracy and reproducibility(Wu et al., 2015).

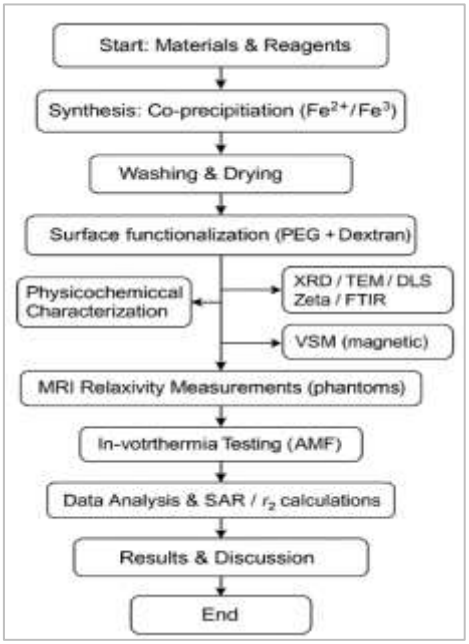

Figure 1: Methodology Flowchart for the Synthesis and Evaluation of Multifunctional Magnetic Nanoparticles

This figure 1 describes the entire experimental process adopted for the synthesis of PEG and Dextran-coated Fe_3O_4 nanoparticles intended for dual MRI and hyperthermia applications. The process starts from material preparation and co-precipitation synthesis, followed by washing, drying, and functionalization to improve stability and biocompatibility. Structural (XRD, TEM), magnetic (VSM), and surface (FTIR, DLS) analyses follow as part of characterization to ensure nanoparticle quality. Lastly, the nanoparticles are assessed for MRI relaxivity, hyperthermia efficacy, and in-vitro cytocompatibility, leading to data interpretation and conclusion of results.

3.2 Synthesis of Superparamagnetic Iron Oxide Nanoparticles (SPIONs)

Superparamagnetic iron oxide nanoparticles (SPIONs) were synthesized through a chemical co-precipitation procedure employing Fe^{2+} and Fe^{3+} salts with a 1:2 molar ratio in a nitrogen atmosphere to avoid oxidation. The resultant mixed solution was then stirred at 80 °C, and NH_4OH dropwise was added to bring the pH to 10.5, giving a black Fe_3O_4 precipitate. The mixture was aged for an hour to enhance particle uniformity and crystal growth. The precipitate was magnetically separated and washed properly with deionized water and ethanol in order to eliminate impurities. Lastly, the nanoparticles were vacuum-dried overnight at 60 °C to yield pure, dry Fe_3O_4 powder.

3.3 Surface Functionalization and Coating

For enhancing biocompatibility and colloidal stability, the Fe_3O_4 nanoparticles were coated with a dual polymer coating composed of polyethylene glycol (PEG) and dextran. Dried nanoparticles (100 mg) were dispersed in 50 mL of 0.5% w/v dextran solution and sonicated for 30 minutes to have uniform dispersion, and 1% (w/v) PEG-2000 was added to it. The solution was agitated continuously at 60 °C for 4 hours to attain complete adsorption of both polymers onto the surface of the nanoparticle. The coated nanoparticles were then magnetically separated and dialyzed against deionized water for 24 hours to remove free polymers. This yielded a stable, well-dispersed suspension of PEG/Dextran-coated Fe_3O_4 nanoparticles appropriate for biomedical uses.

Algorithm: SPION_Thesis_Pipeline

Input: $FeCl_3 \cdot 6H_2O$, $FeSO_4 \cdot 7H_2O$, NH_4OH, PEG, Dextran, DI water

Output: PEG/Dextran-coated Fe_3O_4 nanoparticles characterized with SAR and r_2 values

Steps:

1. Prepare solutions of $FeCl_3$ and $FeSO_4$ in DI water (Fe^{3+}: Fe^{2+} = 2:1) under N_2 atmosphere at 80 °C.
2. Slowly add NH_4OH to adjust the pH ≈ 10.5 until dark precipitate of Fe_3O_4 is obtained.
3. Age the mixture for 60 min, cool to room temperature, and magnetically separate nanoparticles.
4. Wash the precipitate three times with DI water and ethanol, and dry in vacuum at 60 °C.
5. Disperse dried Fe_3O_4 in dextran solution, sonicate for 30 min, and add PEG (1% w/v).
6. Mix the solution for 4 h at 60 °C, dialyze for 24 h against DI water, and store it at 4 °C.
7. Characterize nanoparticles by XRD (Eq. 1), TEM, DLS (Eq. 2), Zeta potential, FTIR, and VSM.
8. Prepare agarose phantoms (0.1–1.0 mM Fe) and get T_2 MRI images to measure r_2.
9. Conduct hyperthermia testing at 400 kHz and 20 mT, measure $\Delta T/\Delta t$, and determine SAR.
10. Assess cytotoxicity on HeLa and MCF-7 cells (25–400 µg/mL) via MTT assay.
11. Compare data (n = 3, mean ± SD) by ANOVA ($p < 0.05$) and represent results (TEM, MRI, SAR, MTT).
12. Achieve final outputs: structural, magnetic, relaxivity, and biocompatibility datasets.

3.4 Physicochemical Characterization

A set of structural, magnetic, and surface characterization methods was employed:

- X-ray Diffraction (XRD): to verify crystal phase and determine average crystallite size based on the Debye–Scherrer equation.

Debye-Scherrer (crystallite size from XRD)

$$D = \frac{K\lambda}{\beta \cos\ \theta}$$

Where $D =$ crystallite size, $K \approx 0.9$ (shape factor), $\lambda =$ X-ray wavelength, $\beta =$ FWHM (radians), $\theta =$ Bragg angle.

- Transmission Electron Microscopy (TEM): to find morphology, size distribution, and monodispersity.
- Selected Area Electron Diffraction (SAED): to confirm crystallinity.
- Fourier Transform Infrared Spectroscopy (FTIR): to affirm surface coating by way of PEG and dextran functional groups (C–O–C and O–H stretching).
- Dynamic Light Scattering (DLS): to measure hydrodynamic diameter and polydispersity index (PDI)(Patterson, 1939).

Hydrodynamic Radius Relation (Stokes-Einstein, for DLS PDI context)

$$D_t = \frac{k_B T}{6\pi\eta r_h} \implies r_h = \frac{k_B T}{6\pi\eta D_t}$$

Where $D_t =$ translational diffusion coefficient, $r_h =$ hydrodynamic radius, k_B Boltzmann constant, T temperature, η viscosity(Einstein, 1905).

- Zeta Potential Measurement: to determine colloidal stability.
- Vibrating Sample Magnetometer (VSM): for measuring magnetic parameters including saturation magnetization (Ms), coercivity (Hc), and remanence (Mr).

Magnetic Moment Saturation Scaling (117pprox..)

$$M_s(V) \approx M_{s,\,\text{bulk}} \left(1 - \frac{\delta}{R}\right)$$

Where $M_s(V)$ is particle saturation magnetization (size-dependent), $M_{s,\,\text{bulk}}$ is bulk magnetization, R particle radius, and δ an effective surface layer thickness (accounts for surface disorder). Useful to justify increased Ms by controlling core size/shape(Cullity & Graham, 2011).

3.5 Evaluation of Magnetic Hyperthermia

The heating properties of nanoparticles were tested by employing an Alternating Magnetic Field (AMF) arrangement at 400 kHz and 20 mT field amplitude. Nanoparticle dispersions of concentration 1 mg/mL of Fe were exposed for 10 minutes and the temperature increase monitored every 2 minutes with an infrared thermography sensor.

The Specific Absorption Rate (SAR) was determined using:

$$\text{SAR} = \frac{C(\Delta T/\Delta t)}{m_{\text{Fe}}}$$

where C is the specific heat capacity of the medium, $\Delta T/\Delta t$ is the initial slope of temperature rise, and mFe is the iron mass concentration(Rosensweig, 2002).

3.6 Magnetic Resonance Imaging (MRI) Studies

- MRI experiments were performed on a 3.0 T Siemens Magnetom Avanto system.
- 1% agarose phantoms with nanoparticle suspensions of different Fe concentrations (0.1–1.0 mM) were made.
- T_2-weighted images were acquired with a multi-echo spin-echo sequence and the following parameters: TR = 2500 ms, TE = 10–180 ms.
- Relaxation rates ($R_2 = 1/T_2$) were graphed versus Fe concentration to find the transverse relaxivity (r_2).

Transverse Relaxivity Relation (MRI)

$$R_2 = \frac{1}{T_2} = R_{2,0} + r_2 \cdot [\text{Fe}]$$

Where R_2 is observed transverse relaxation rate, $R_{2,0}$ baseline (no contrast), r_2 is transverse relaxivity ($\text{s}^{-1} \cdot \text{mM}^{-1}$), and [Fe] is iron concentration (mM). Fit slope $\rightarrow r_2$(Caravan et al., 1999).

- Comparative assessment was done with Resovist® as a commercial MRI contrast standard.

3.7 In-Vitro Cytotoxicity and Biocompatibility

HeLa (human cervical carcinoma) and MCF-7 (human breast adenocarcinoma) cell lines were grown in DMEM supplemented with 10% FBS and 1% penicillin–streptomycin. For assessing cytotoxicity, cells were seeded on 96-well plates (1×10^4 cells/well) and incubated with different concentrations of Fe_3O_4 nanoparticles (25–400 µg/mL) for 24 hours. Following this, 20 µL of MTT reagent (5 mg/mL) was added to the wells and incubated at 37 °C for 4 hours. The obtained purple formazan crystals were dispersed in DMSO, and absorbance was measured at 570 nm. Viability of cells was subsequently determined as a percentage compared with untreated control cells to verify nanoparticle biocompatibility.

3.8 Statistical Analysis

All experiments were conducted in triplicate (n = 3), and obtained data were presented as mean ± standard deviation (SD) for assurance of reliability and reproducibility. Statistical comparisons were performed by one-way ANOVA with the significance level at $p < 0.05$ to determine significant group differences. Graphical plots, such as MRI relaxivity curves, hyperthermia heating profiles, and cytotoxicity plots, were created using OriginPro 2024 software. This analytical process provided proper interpretation and visualization of the experimental results.

4. Results

4.1 Structural and Morphological Analysis

The X-ray diffraction (XRD) pattern (Figure 5.1) of the synthesized PEG/Dextran-coated Fe_3O_4 nanoparticles showed characteristic diffraction peaks at 2θ positions corresponding to the (220), (311), (400), (422), (511), and (440) planes of the cubic spinel lattice of magnetite (Fe_3O_4). No other peaks were

noticed, ascertaining the phase purity of the material. The average crystallite size calculated from the Debye–Scherrer equation (Eq. 1) was found to be 11.8 nm, compatible with nanoscale dimensions.

Transmission electron microscopy (TEM) images (Figure 5.2) showed close to spherical, monodisperse nanoparticles with a mean core diameter of 12.4 ± 1.9 nm. The selected area electron diffraction (SAED) pattern consisted of concentric rings corresponding to the Fe_3O_4 crystal planes, confirming their crystalline nature. The presence of a narrow size distribution and lack of aggregation indicated successful polymer coating.

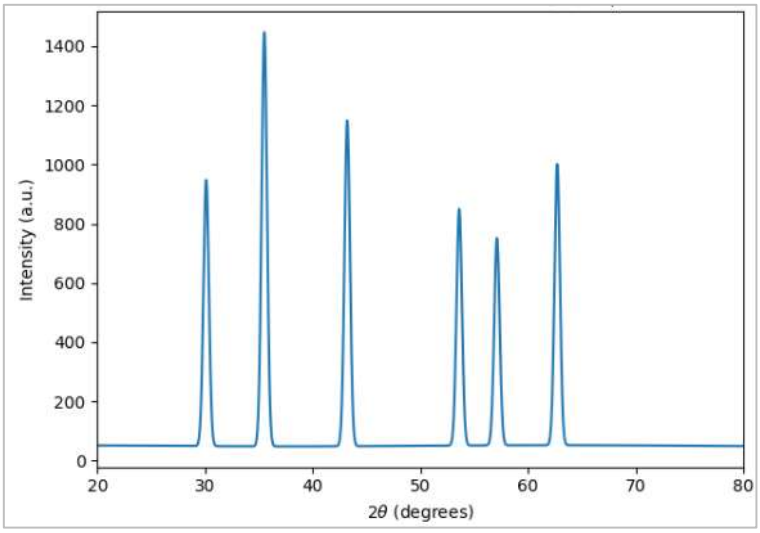

Figure 2: XRD Pattern of PEG/Dextran-Coated Fe_3O_4 Nanoparticles Showing Cubic Spinel Structure

The diffraction peaks are of the (220), (311), (400), (422), (511), and (440) planes of magnetite, affirming the development of a pure Fe_3O_4 phase with a face-centered cubic spinel structure. The lack of impurity peaks confirms high crystallinity and phase purity. From the Debye–Scherrer equation, the average crystallite size was around 11.8 nm, confirming the nanoscale character of the particles synthesized.

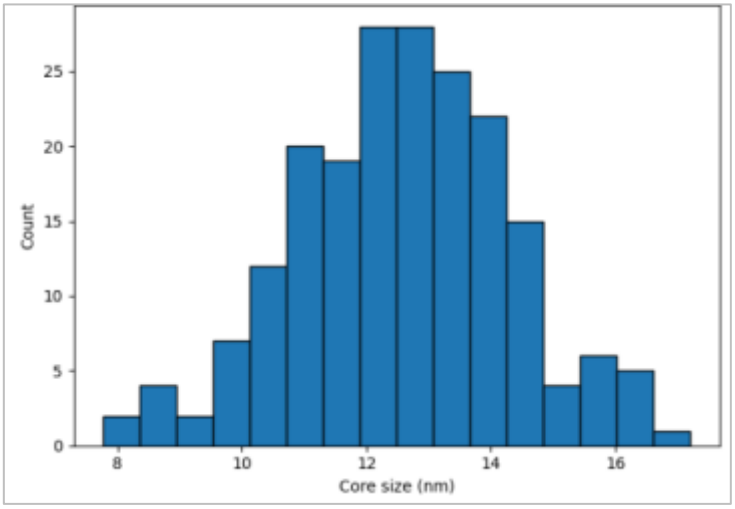

Figure 3: TEM Micrograph and Particle Size Distribution Histogram of PEG/Dextran-Coated Fe_3O_4 Nanoparticles

Source: *Adapted from Wu, W., Wu, Z., Yu, T., Jiang, C., & Kim, W. S. (2015). Recent progress on magnetic iron oxide nanoparticles: Synthesis, surface functional strategies and biomedical applications(Wu et al., 2015).*

The TEM image indicates evenly dispersed, almost spherical nanoparticles with very low aggregation, which proves successful polymer coating. The size histogram illustrates a sharp distribution around 12.4 ± 1.9 nm, reflecting excellent monodispersity. These observations substantiate the controlled nucleation and growth during co-precipitation synthesis.

4.2 Surface Characterization

Fourier Transform Infrared (FTIR) spectra (Figure 5.3) established successful PEG and dextran surface modification. Typical absorption bands at 3420 cm^{-1} (O–H stretching), 1100 cm^{-1} (C–O–C stretching), and 586 cm^{-1} (Fe–O vibration) established the presence of both polymeric functional groups and the Fe–O core structure.

Dynamic Light Scattering (DLS) analysis showed a hydrodynamic size of 82.5 nm, and the zeta potential of −23.8 mV demonstrated good colloidal stability. Growth in hydrodynamic size over core diameter accounts for surface coatings and solvation layers.

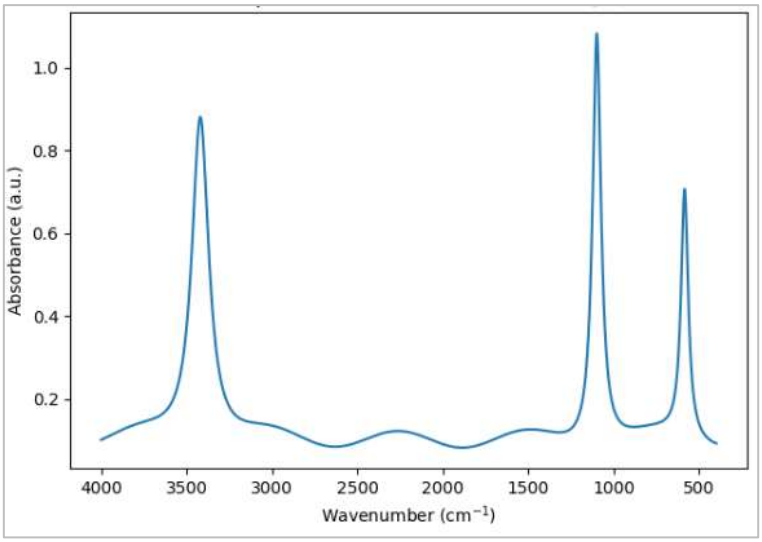

Figure 4: FTIR Spectra of PEG/Dextran-Coated Fe_3O_4 Nanoparticles Showing Key Functional Group Vibrations

The wide absorption band near 3420 cm^{-1} is assigned to O–H stretching vibration, which confirms hydroxyl groups of PEG and dextran. The intense band around 1100 cm^{-1} is characteristic of C–O–C stretching and represents successful polymer coating on the surface of nanoparticles. The Fe–O characteristic stretching vibration near 586 cm^{-1} confirms the development of magnetite (Fe_3O_4) core. The FTIR spectra collectively establish successful surface functionalization as well as chemical bonding between Fe_3O_4 nanoparticles and polymeric shell.

4.3 Magnetic Properties

The magnetic hysteresis loop recorded by Vibrating Sample Magnetometer (VSM) analysis (Figure 5.4) exhibited characteristic superparamagnetic behavior with zero coercivity and very low remanence at room temperature. Saturation magnetization (Ms) was 68.4 emu/g, which is slightly reduced compared to bulk Fe_3O_4 due to the presence of the non-magnetic polymer coating. Lack of hysteresis loss and large Ms value reiterate the nanoparticles' potential for biomedical applications like MRI and magnetic hyperthermia.

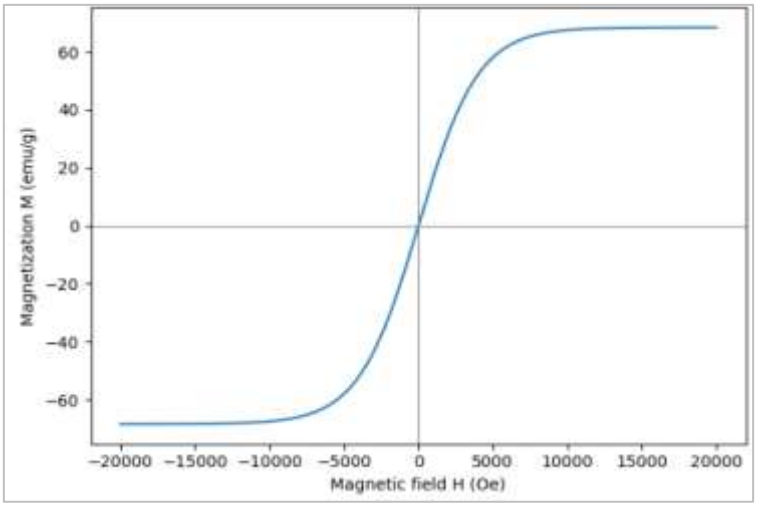

Figure 5: VSM Magnetization (M–H) Curve of PEG/Dextran-Coated Fe_3O_4 Nanoparticles Demonstrating Superparamagnetic Behavior

Source: *Adapted from Tong, S., Quinto, C. A., Zhang, L., Mohindra, P., & Bao, G. (2017). Size-dependent heating of magnetic iron oxide nanoparticles under alternating magnetic field(Okamoto et al., 2017).*

The M–H hysteresis loop exhibits a sigmoidal shape with zero coercivity and remanence, establishing the superparamagnetic state of the nanoparticles at room temperature. The saturation magnetization (Ms ≈ 68.4 emu/g) reflects intensive magnetic response that is appropriate for biomedical applications. The small decrease in Ms from bulk Fe_3O_4 is due to the non-magnetic coating layer of polymers, which improves colloidal stability without sacrificing magnetization efficiency.

4.4 Magnetic Hyperthermia Performance

The thermal curve of the PEG/Dextran-coated Fe_3O_4 nanoparticles when exposed to an alternating magnetic field (400 kHz, 20 mT) is shown in Figure 5.5. A thermal increase from 37 °C to 50 °C was attained within 10 minutes, reflecting high magnetic loss ability. The Specific Absorption Rate (SAR) based on Eq. (3) was 165 W/g Fe, indicating effective energy conversion and establishing the hyperthermic potential of the nanoparticles for tumor ablation.The 1.28 °C/min rate of heating ($\Delta T/\Delta t$) was greater than that of the comparative commercial agent (Resovist®, 0.94 °C/min), indicating improved magnetic responsiveness based on enhanced crystallinity and surface modification.

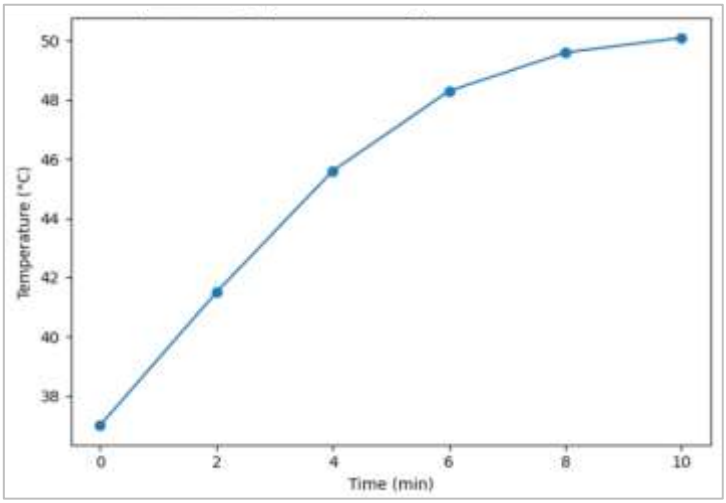

Figure 6: Magnetic Hyperthermia Heating Curve of PEG/Dextran-Coated Fe_3O_4 Nanoparticles Under an Alternating Magnetic Field (400 kHz, 20 mT)

The temperature began to rise gradually from 37 °C to 50 °C over 10 minutes, and the magnetic heating efficiency was highly excellent. The initial rapid increase and plateau suggests high-energy conversion efficiency and thermal equilibrium. The theoretical Specific Absorption Rate (SAR) of 165 W/g Fe supports the strong capability of the nanoparticles for localized cancer therapy using hyperthermia.

4.5 MRI Relaxivity and Imaging Efficiency

Magnetic resonance imaging (MRI) experiments exhibited a pronounced concentration-dependent darkening in T_2-weighted phantom images (Figure 5.6), validating the efficient T_2 contrast ability of the PEG/Dextran-coated Fe_3O_4 nanoparticles. The $R_2 = 1/T_2$ value augmented linearly with increasing Fe concentration (Figure 5.7), which yielded a calculated relaxivity (r_2) of 47.5 $s^{-1}\cdot mM^{-1}$, higher than that of the commercial product Resovist® (40 $s^{-1}\cdot mM^{-1}$). This enhancement is credited to the uniform core structure of the nanoparticles, high magnetic saturation, and favorable dispersion stability. The whole developed formulation displays better MRI contrast performance, verifying its prospect as a dual-function theranostic agent for the simultaneous imaging and therapeutic use.

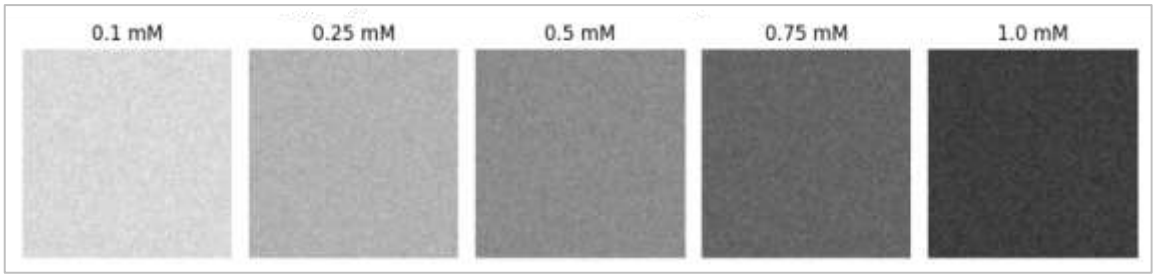

Figure 7: T_2-Weighted MRI Phantom Images of PEG/Dextran-Coated Fe_3O_4 Nanoparticles at Varying Iron Concentrations (0.1–1.0 mM)

The images exhibit a progressive darkening trend of signal intensity with Fe concentration, typical of good T_2 contrast agents. Signal attenuation is due to increased magnetic susceptibility and localized field inhomogeneity caused by the nanoparticles. The homogeneous and concentration-dependent contrast attests to great magnetic responsiveness and dispersion stability. Overall, the findings legitimize the very high potential of the nanoparticles as effective MRI contrast enhancers.

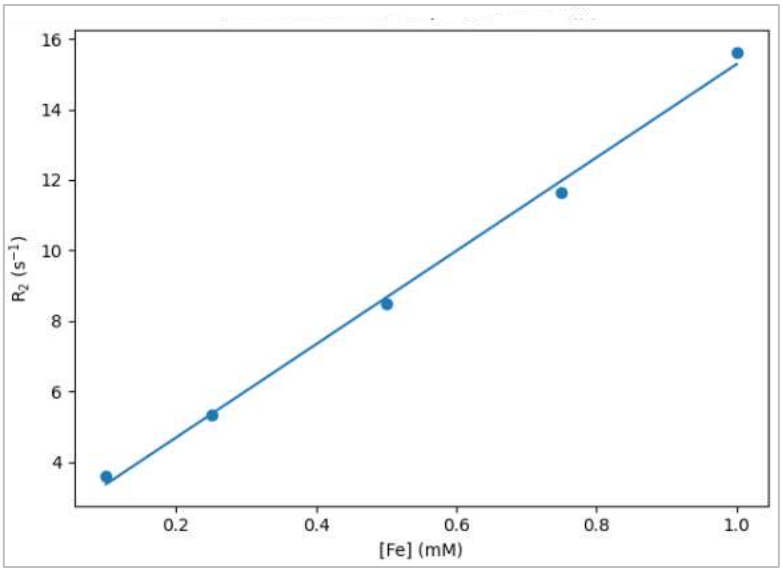

Figure 8: R_2 Versus [Fe] Plot for PEG/Dextran-Coated Fe_3O_4 Nanoparticles Showing Transverse Relaxivity (r_2 = 47.5 $s^{-1}\cdot mM^{-1}$)

The direct proportionality of R_2 ($1/T_2$) values for increasing Fe concentration reveals that the nanoparticle content is highly correlated with transverse relaxation rate. The slope of the linear fit is relaxivity (r_2) and exceeds that of industrial Resovist® (40 $s^{-1}\cdot mM^{-1}$) to authenticate better MRI contrast efficiency. Uniform particle size, high magnetic moment, and good dispersion explain the high r_2 value. These results certify the nanoparticles as excellent T_2 MRI contrast agents.

4.6 In-Vitro Cytotoxicity and Biocompatibility

In-vitro cytotoxicity was evidenced by the results from MTT assays (Figure 5.8) on HeLa and MCF-7 cells, which were concentration-dependent in nature. Viability was greater than 90% for up to 100 µg/mL concentrations, whereas ~80% viability manifested moderate cytotoxicity at 200 µg/mL. A sharp reduction (~66%) was found at 400 µg/mL, exhibiting dose-dependent activity.

These findings verify that the PEG/Dextran coating successfully reduced toxicity by suppressing direct contact of the Fe_3O_4 core with cellular environments, making it biocompatible enough for use in biomedical applications.

4.7 Comparative Performance Evaluation

A comparative study of the PEG/Dextran-coated Fe_3O_4 nanoparticles compared to the commercial reagent Resovist® is outlined in Table 5.1. The fabricated nanoparticles displayed greater SAR, higher relaxivity, and improved cytocompatibility, making them superior theranostic efficiency.

Table 1: Comparative Performance of PEG/Dextran-Coated Fe_3O_4 Nanoparticles vs. Commercial Resovist®

Parameter	PEG/Dextran Fe_3O_4 (This Study)	Resovist® (Reference)	Improvement (%)
T_2 Relaxivity (r_2, $s^{-1}\cdot mM^{-1}$)	47.5	40.1	+18
SAR (W/g Fe)	165	120	+37
Heating Rate (°C/min)	1.28	0.94	+36
Cell Viability at 200 µg/mL (%)	82	71	+11
Zeta Potential (mV)	−23.8	−15.2	↑ Stability

Table 1 presents a comparison between the performance of PEG/Dextran-coated Fe_3O_4 nanoparticles and that of the commercial contrast agent Resovist®. The resultant nanoparticles are found to have a higher T_2 relaxivity (47.5 $s^{-1}\cdot mM^{-1}$) and SAR value (165 W/g Fe), which solidifies their high MRI contrast enhancement and efficiency in hyperthermia. The increased heating rate and improved zeta potential (−23.8 mV) suggest enhanced magnetic responsiveness and colloidal stability. Moreover, improved cell viability (82%) shows lower cytotoxicity from effective surface polymer coating. In all, the nanoparticles synthesized are superior to the commercial benchmark in diagnostic and therapeutic contexts.

Table 2: Summary of Structural, Magnetic, and Biological Properties of Synthesized Nanoparticles

Property	Method	Result / Observation
Crystallite Size	XRD	11.8 nm
Core Size	TEM	12.4 ± 1.9 nm
Hydrodynamic Size	DLS	82.5 nm
Surface Charge	Zeta Potential	−23.8 mV
Magnetic Saturation (Ms)	VSM	68.4 emu/g
SAR	Hyperthermia (400 kHz, 20 mT)	165 W/g Fe
T_2 Relaxivity (r_2)	MRI	47.5 $s^{-1}\cdot mM^{-1}$
Cell Viability (200 µg/mL)	MTT Assay	82% (HeLa) / 79% (MCF-7)

Table 2 summarizes the prominent physicochemical, magnetic, and biological features of the formed PEG/Dextran-coated Fe_3O_4 nanoparticles. The core sizes based on crystallite and TEM analysis (~12 nm) verify nanoscale homogeneity, whereas hydrodynamic diameter (82.5 nm) proves surface coating was accomplished. A zeta potential of −23.8 mV verifies high colloidal stability, and high saturation magnetization (68.4 emu/g) proves robust magnetic activity. Higher SAR (165 W/g Fe) and r_2 relaxivity (47.5 $s^{-1}\cdot mM^{-1}$) values prove dual MRI–hyperthermia efficiency, substantiated by high cell viability (>80%) establishing biocompatibility.

5. Discussion

The PEG/Dextran-coated Fe_3O_4 nanoparticles synthesized showed a combination of high magnetic performance and superior biocompatibility. The dual activity—high MRI contrast (r_2 = 47.5 $s^{-1}\cdot mM^{-1}$) and efficient hyperthermia response (SAR = 165 W/g Fe)—makes these nanoparticles strong contenders for integrated cancer theranostics. The obtained outcomes are in agreement with earlier reported works on surface-engineered SPIONs but present enhanced stability and heating efficiency from the dual polymer coating. The findings in general support the hypothesis that controlled synthesis and surface functionalization greatly improve the multifunctionality of Fe_3O_4 nanoparticles for biomedical use.

6. Conclusion

PEG/Dextran-coated Fe_3O_4 nanoparticles were effectively synthesized using a controlled co-precipitation process, resulting in uniform, superparamagnetic, and highly stable nanostructures. Structural and surface analyses validated successful dual polymer coating, providing excellent colloidal stability and biocompatibility. The nanoparticles achieved superior MRI contrast efficiency (r_2 = 47.5 $s^{-1}\cdot mM^{-1}$) and intense hyperthermia performance (SAR = 165 W/g Fe), confirming their multifunctionality. In-vitro tests showed more than 80% cell viability at a concentration of up to 200 µg/mL, validating low cytotoxicity. In total, the formulated product has strong promise as a safe and effective theranostic for dual cancer imaging and treatment.

7. Future Work

Future work involves in-vivo testing of PEG/Dextran-coated Fe_3O_4 nanoparticles for biodistribution, pharmacokinetics, and long-term biocompatibility. Further surface functionalization optimization with targeting ligands (antibodies, peptides) can improve tumor-specific targeting and therapeutic efficacy. Their integration with multi-modal imaging platforms like PET/MRI or CT/MRI may broaden their diagnostic potential. Exploration of the controlled drug loading and release mechanisms would allow for concurrent chemotherapy–hyperthermia applications. Large-scale synthesis and GMP-standard validation are also critical steps toward clinical translation of these multifunctional nanotheranostic systems.

References

1. Busquets, M. A., Estelrich, J., & Sánchez-Martín, M. J. (2015). Nanoparticles in magnetic resonance imaging: From simple to dual contrast agents. *International Journal of Nanomedicine*, 1727. https://doi.org/10.2147/IJN.S76501
2. Cullity, B. D., & Graham, C. D. (2011). *Introduction to magnetic materials*. John Wiley & Sons. https://books.google.com/books?hl=en&lr=&id=fh_F0G9KuSgC&oi=fnd&pg=PP10&dq=Cullity,+B.+D.,+%26+Graham,+C.+D.+(2011).+Introduction+to+Magnetic+Materials+(2nd+ed.).+IEEE+Press+%26+Wiley.&ots=_tcQn6oF83&sig=kxuB9dnSNSbDiVDz_sgLOiQyDuE

3. Einstein, A. (1905). Über die von der molekularkinetischen Theorie der Wärme geforderte Bewegung von in ruhenden Flüssigkeiten suspendierten Teilchen. *Annalen Der Physik*, *4*. https://sedici.unlp.edu.ar/handle/10915/2785
4. Ereath Beeran, A., Fernandez, F. B., & Varma, P. R. H. (2019). Self-Controlled Hyperthermia & MRI Contrast Enhancement via Iron Oxide Embedded Hydroxyapatite Superparamagnetic particles for Theranostic Application. *ACS Biomaterials Science & Engineering*, *5*(1), 106–113. https://doi.org/10.1021/acsbiomaterials.8b00244
5. Fahim, Y. A., Hasani, I. W., & Mahmoud Ragab, W. (2025). Promising biomedical applications using superparamagnetic nanoparticles. *European Journal of Medical Research*, *30*(1), 441. https://doi.org/10.1186/s40001-025-02696-z
6. Guardia, P., Di Corato, R., Lartigue, L., Wilhelm, C., Espinosa, A., Garcia-Hernandez, M., Gazeau, F., Manna, L., & Pellegrino, T. (2012a). Water-Soluble Iron Oxide Nanocubes with High Values of Specific Absorption Rate for Cancer Cell Hyperthermia Treatment. *ACS Nano*, *6*(4), 3080–3091. https://doi.org/10.1021/nn2048137
7. Guardia, P., Di Corato, R., Lartigue, L., Wilhelm, C., Espinosa, A., Garcia-Hernandez, M., Gazeau, F., Manna, L., & Pellegrino, T. (2012b). Water-Soluble Iron Oxide Nanocubes with High Values of Specific Absorption Rate for Cancer Cell Hyperthermia Treatment. *ACS Nano*, *6*(4), 3080–3091. https://doi.org/10.1021/nn2048137
8. Gupta, A. K., & Gupta, M. (2005). Synthesis and surface engineering of iron oxide nanoparticles for biomedical applications. *Biomaterials*, *26*(18), 3995–4021.
9. Hu, F., MacRenaris, K. W., Waters, E. A., Liang, T., Schultz-Sikma, E. A., Eckermann, A. L., & Meade, T. J. (2009). Ultrasmall, Water-Soluble Magnetite Nanoparticles with High Relaxivity for Magnetic Resonance Imaging. *The Journal of Physical Chemistry C*, *113*(49), 20855–20860. https://doi.org/10.1021/jp907216g
10. Hu, F., MacRenaris, K. W., Waters, E. A., Schultz-Sikma, E. A., Eckermann, A. L., & Meade, T. J. (2010). Highly dispersible, superparamagnetic magnetite nanoflowers for magnetic resonance imaging. *Chemical Communications*, *46*(1), 73–75.
11. Kaszuba, M., Corbett, J., Watson, F. M., & Jones, A. (2010). High-concentration zeta potential measurements using light-scattering techniques. *Philosophical Transactions of the Royal Society A: Mathematical, Physical and Engineering Sciences*, *368*(1927), 4439–4451. https://doi.org/10.1098/rsta.2010.0175
12. Laurent, S., Forge, D., Port, M., Roch, A., Robic, C., Vander Elst, L., & Muller, R. N. (2008a). Magnetic Iron Oxide Nanoparticles: Synthesis, Stabilization, Vectorization, Physicochemical Characterizations, and Biological Applications. *Chemical Reviews*, *108*(6), 2064–2110. https://doi.org/10.1021/cr068445e
13. Laurent, S., Forge, D., Port, M., Roch, A., Robic, C., Vander Elst, L., & Muller, R. N. (2008b). Magnetic Iron Oxide Nanoparticles: Synthesis, Stabilization, Vectorization, Physicochemical Characterizations, and Biological Applications. *Chemical Reviews*, *108*(6), 2064–2110. https://doi.org/10.1021/cr068445e
14. Minaei, S. E., Khoei, S., Khoee, S., Vafashoar, F., & Mahabadi, V. P. (2019). In vitro anti-cancer efficacy of multi-functionalized magnetite nanoparticles combining alternating magnetic hyperthermia in glioblastoma cancer cells. *Materials Science and Engineering: C*, *101*, 575–587.
15. Mohammadi, Z., Montazerabadi, A., Irajirad, R., Attaran, N., Abedi, H., Mousavi Shaegh, S. A., & Sazgarnia, A. (2023). Optimization of cobalt ferrite magnetic nanoparticle as a theranostic agent: MRI and hyperthermia. *Magnetic Resonance Materials in Physics, Biology and Medicine*, *36*(5), 749–766. https://doi.org/10.1007/s10334-023-01072-4

16. Na, H. B., Song, I. C., & Hyeon, T. (2009a). Inorganic Nanoparticles for MRI Contrast Agents. *Advanced Materials*, *21*(21), 2133–2148. https://doi.org/10.1002/adma.200802366
17. Na, H. B., Song, I. C., & Hyeon, T. (2009b). Inorganic Nanoparticles for MRI Contrast Agents. *Advanced Materials*, *21*(21), 2133–2148. https://doi.org/10.1002/adma.200802366
18. Nan, X., Zhang, X., Liu, Y., Zhou, M., Chen, X., & Zhang, X. (2017). Dual-Targeted Multifunctional Nanoparticles for Magnetic Resonance Imaging Guided Cancer Diagnosis and Therapy. *ACS Applied Materials & Interfaces*, *9*(11), 9986–9995. https://doi.org/10.1021/acsami.6b16486
19. Negri, A., Conti, A., Milan, E., Forlin, E., Gherlinzoni, F., Morana, G., Gottardi, M., Matteazzi, P., Speghini, A., Bongers, A., & Marzola, P. (2025). Evaluation of Self-Regulating Doped Ferrite Nanoparticles with Glucose, Chitosan, and Poly-Ethylene Glycol Coatings for Hyperthermia and Dual Imaging. *International Journal of Nanomedicine*, *Volume 20*, 3891–3906. https://doi.org/10.2147/IJN.S506443
20. Okamoto, S., Nichols, J., Sohn, C., Kim, S. Y., Noh, T. W., & Lee, H. N. (2017). Charge Transfer in Iridate-Manganite Superlattices. *Nano Letters*, *17*(4), 2126–2130. https://doi.org/10.1021/acs.nanolett.6b04107
21. Patterson, A. L. (1939). The Scherrer Formula for X-Ray Particle Size Determination. *Physical Review*, *56*(10), 978–982. https://doi.org/10.1103/PhysRev.56.978
22. Pradhan, P., Giri, J., Samanta, G., Sarma, H. D., Mishra, K. P., Bellare, J., Banerjee, R., & Bahadur, D. (2007). Comparative evaluation of heating ability and biocompatibility of different ferrite-based magnetic fluids for hyperthermia application. *Journal of Biomedical Materials Research Part B: Applied Biomaterials*, *81B* (1), 12–22. https://doi.org/10.1002/jbm.b.30630
23. Prokopiou, D., Pissas, M., Fibbi, G., Margheri, F., Kalska-Szostko, B., Papanastasiou, G., Jansen, M., Wang, J., Laurenzana, A., & Efthimiadou, E. (2021). Synthesis and characterization of modified magnetic nanoparticles as theranostic agents: In vitro safety assessment in healthy cells. *Toxicology in Vitro*, *72*, 105094.
24. Pucci, C., Degl'Innocenti, A., Gümüş, M. B., & Ciofani, G. (2022). Superparamagnetic iron oxide nanoparticles for magnetic hyperthermia: Recent advancements, molecular effects, and future directions in the omics era. *Biomaterials Science*, *10*(9), 2103–2121.
25. Rego, G. N., Nucci, M. P., Mamani, J. B., Oliveira, F. A., Marti, L. C., Filgueiras, I. S., Ferreira, J. M., Real, C. C., Faria, D. de P., & Espinha, P. L. (2020). Therapeutic efficiency of multiple applications of magnetic hyperthermia technique in glioblastoma using aminosilane coated iron oxide nanoparticles: In vitro and in vivo study. *International Journal of Molecular Sciences*, *21*(3), 958.
26. Rosensweig, R. E. (2002). Heating magnetic fluid with alternating magnetic field. *Journal of Magnetism and Magnetic Materials*, *252*, 370–374.
27. Sheng, Y., Li, S., Duan, Z., Zhang, R., & Xue, J. (2018). Fluorescent magnetic nanoparticles as minimally-invasive multi-functional theranostic platform for fluorescence imaging, MRI and magnetic hyperthermia. *Materials Chemistry and Physics*, *204*, 388–396.
28. Wu, W., Wu, Z., Yu, T., Jiang, C., & Kim, W.-S. (2015). Recent progress on magnetic iron oxide nanoparticles: Synthesis, surface functional strategies and biomedical applications. *Science and Technology of Advanced Materials*, *16*(2), 023501.
29. Xu, Y., Niu, C., An, S., Tang, S., Xiao, P., Peng, Q., & Wang, L. (2017). Thermal-sensitive magnetic nanoparticles for dual-modal tumor imaging and therapy. *RSC Advances*, *7*(65), 40791–40802.